Journal of Materials Research and Technology 34 (2025) 730–737

Contents lists available at ScienceDirect

Journal of Materials Research and Technology

journal homepage: www.elsevier.com/locate/jmrt

Transformation induced plasticity (TRIP) due to precipitation during continuous tempering of quenched and tempered steels

Niki Nouri *, Elena Hillenmeyer, Thanusan Thavarajan, Stefan Dietrich, Volker Schulze

Institute for Applied Materials – Materials Science and Engineering (IAM-WK), Karlsruhe Institute of Technology, Karlsruhe, Germany

ARTICLE INFO

Keywords:
Transformation induced plasticity
Tempering
Quenched and tempered steels
Precipitation
Carbide fraction

ABSTRACT

Heat treatment is an essential step in achieving the desired characteristics in steels. Quenched and tempered (Q&T) steels are often tempered to adjust the strength-ductility ratio by taking advantage of the precipitation of carbides. In practice, many parts already contain residual stresses, for example due to the temperature gradients during surface hardening, and therefore tempering takes place under the influence of these stresses. The occurring transformation induced plasticity (TRIP) means significant plastic deformation during a phase transformation under a stress below the material's yield strength. In this work, tempering TRIP of three different Q&T steels has been studied by means of dilatometry, hardness measurements, and scanning electron microscopy. The heating rate, as well as the direction and level of applied stress, have been varied. The results have proven the existence of TRIP strain during continuous tempering and its linear dependence on the fraction of the precipitates. A higher amount of carbon results in a growth of the precipitates surface area percentage, leading to an increase in the TRIP strain and consequently the TRIP constant. This indicates the presence of the Greenwood–Johnson effect, which relates TRIP to the difference in volume between the existing and forming phases.

1. Introduction

1.1. Transformation induced plasticity (TRIP)

The majority of steels require the proper heat treatment (HT) depending on the part, its application and art of fabrication. The HT for quenched and tempered (Q&T) steels consists of a first austenitization and quenching step to create a fully martensitic phase, followed by a tempering step, which results in the formation of precipitates. This allows an adjustment of the strength-ductility ratio depending on the requirements. In some cases, only a local HT is necessary; for example gears fabricated out of Q&T steels are typically first induction hardened to achieve a higher strength at the teeth, while keeping the core ductile. The temperature gradient in the part due to the surface HT leads to the formation of residual stresses [1,2]. Consequently, the part is tempered under the influence of said residual stresses. The occurring precipitation can result in the transformation induced plasticity (TRIP), which is defined to be a significant plastic deformation due to a phase transformation under a stress lower than the material's yield strength [3]. TRIP is caused by two effects: firstly, the Greenwood–Johnson effect [4], which is based on the permanent volume adaptation of the more ductile phase due to the volume difference between the existing and the emerging new phase; and secondly, the Magee effect [5], where the forming new phase is oriented in the direction of applied stress and therefore leads to a permanent anisotropic deformation.

1.2. Tempering TRIP

TRIP effect has been extensively investigated for the martensitic, austenitic and bainitic transformations in steels [3]. However, to the authors' knowledge, no systematic studies of TRIP effect during tempering (T-TRIP) under variation of tempering parameters or carbon content have been performed so far. In a previous study [6], only the Q&T steel 42CrMo4 has been investigated regarding T-TRIP up to 500 °C under compression stress, where it could be observed during precipitation. The applied stress has shown to have a direct impact on the amount of T-TRIP strain. Furthermore, the consideration of T-TRIP in HT simulations has proven to be essential in order to correctly predict the material state, especially the development of residual stress, after HT [7]. For this purpose, it is necessary to determine the TRIP constant K, which defines the relationship between TRIP strain ε_{TRIP} and applied stress σ. It has been observed that K is linear up to half of

* Corresponding author.
E-mail address: niki.nouri@kit.edu (N. Nouri).

https://doi.org/10.1016/j.jmrt.2024.12.042
Received 21 November 2024; Accepted 4 December 2024
Available online 12 December 2024
2238-7854/© 2024 The Authors. Published by Elsevier B.V. This is an open access article under the CC BY license (http://creativecommons.org/licenses/by/4.0/).

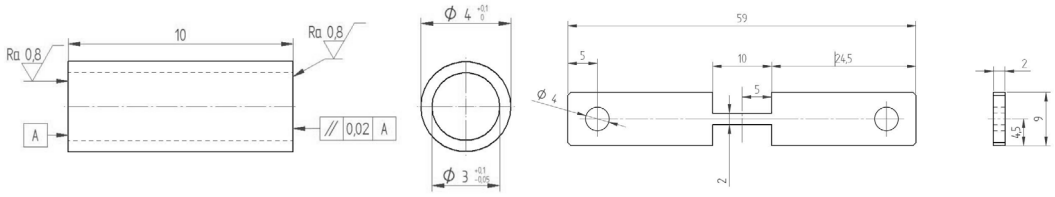

(a) Compression mode (b) Tension mode

Fig. 1. Dilatometric samples.

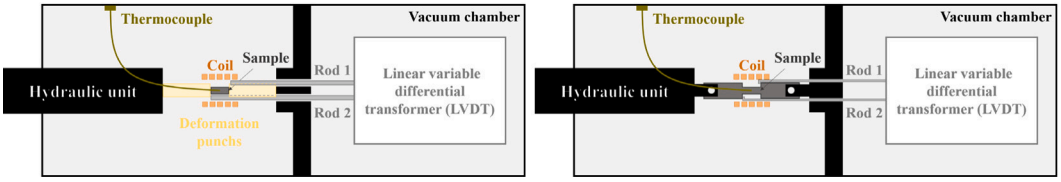

(a) Compression mode (b) Tension mode

Fig. 2. Dilatometer setups.

the yield strength of the softer phase and this linear correlation can be described by the following equation [4]:

$$\varepsilon_{TRIP}(w) = K \cdot \sigma \cdot f(w), \tag{1}$$

with w being the proportion of the transformed phase between 0 and 1, with $f(w = 0) = 0$ and $f(w = 1) = 1$. Thus, the maximum TRIP strain ε_{TRIP}^{max} after tempering and finished precipitation step is equal to $K \cdot \sigma$. Different approaches are suggested in the literature for modeling $f(w)$ [8–13], but these have not been applied to tempering phase transformation yet.

1.3. This work

This work's goal is to further investigate T-TRIP during the precipitation of cementite and identify its relevance in the HT of Q&T steels. Firstly, different dilatometric experiments were conducted on three different steels with a variation in carbon content to measure the length change during tempering. The investigations were carried out under both compression and tension, where different parameters, such as the stress level and the heating rate, were varied. Secondly, the microstructure and precipitates were analyzed after tempering in different samples, using image analysis. Finally, using the results from the steps mentioned above, the dependence between the T-TRIP constant and the variable parameters, as well as the carbon content, was analyzed and discussed.

2. Material and methods

2.1. Material

The Q&T steels listed in Table 1 were chosen to be investigated. All samples were delivered as tempered rods before being machined. These Q&T steels are hardened after austenization at 820–850 °C [14]. While being tempered, they precipitate during the first and third tempering stages [15,16]: in the first tempering stage (100–200 °C) the tetragonal martensite is transformed into cubic martensite and ϵ-carbide ($Fe_{2.4}C$) is precipitated, whereas in the third tempering stage (320–400 °C) the cubic martensite is transformed into ferrite and cementite (Fe_3C) is precipitated. Both stages lead to a volume decrease as well as an increase of ductility.

2.2. Dilatometric heat treatment

Two types of samples were manufactured for the investigations: firstly, round hollow compression samples (Fig. 1(a)), and secondly, flat tensile samples (Fig. 1(b)). A TA Instruments DIL805A/D deformation dilatometer was used for the determination of yield strength, as well as for heat treatments under applied stress and the measurement of the resulting length change.

Table 1
Chemical composition of the investigated Q&T steels in wt-%.

Material	C	Cr	Mo	Mn	Si	Ni	Cu	P	S	Fe
25CrMo4	0.26	0.99	0.18	0.69	0.28	0.15	0.05	0.01	0.001	Bal.
34CrMo4	0.35	1.13	0.29	0.81	0.33	0.14	0.23	0.02	0.002	Bal.
50CrMo4	0.49	1.01	0.20	0.75	0.28	0.20	0.17	0.02	0.028	Bal.

The heat treatment of the samples was performed in the vacuum chamber of the dilatometer, flooded with helium as shielding gas. They were inductively heated while positioned in the middle of a coil. A linear variable differential transformer (LVDT) unit and SiO_2 rods were used to measure the length change. The temperature was recorded with a thermocouple type S, which was welded in the middle of the sample. Helium was also used for quenching sequences. A hydraulic unit is used to apply the compressive and tensile forces. The device setup in both compression and tension mode is schematically depicted in Fig. 2.

Q&T steels may have different compressive and tensile strengths due to the strength differential (SD) effect [17], therefore tensile and compression tests were both performed. For this purpose, the samples were quenched and tempered without any stress. After reaching the tempering temperature T_t, a pre-force of 300 N was applied, followed by a strain rate of 0.01 mm/s for the determination of tensile yield strength σ_{yT} and compression yield strength σ_{yC} at the tempering temperature. The magnitude of SD has been calculated using the following equation:

$$SD = 1 - \left| \frac{\sigma_{yT}}{\sigma_{yC}} \right|. \tag{2}$$

For the investigation of T-TRIP all samples were first heated up to the austenitization temperature T_{aus} and kept there for the time of t_{aus}. Subsequently, they were quenched to room temperature to create a fully martensitic sample. The hardening step was followed by a continuous tempering with a heating rate of 1 °C/s up to the tempering temperature T_t. The stress σ_{max} was applied before starting the tempering sequence and kept constant until reaching T_t. Five stress levels have been investigated: 0, $0.125 \cdot \sigma_y$, $0.25 \cdot \sigma_y$, $0.375 \cdot \sigma_y$ and $0.5 \cdot \sigma_y$. Fig. 3 qualitatively shows the temperature and stress profile during the T-TRIP experiments.

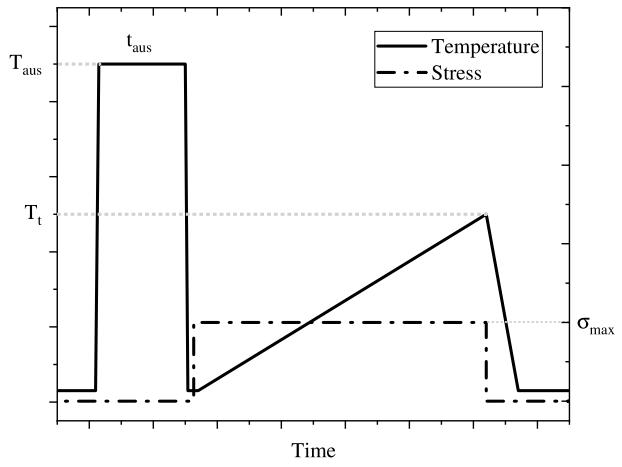

Fig. 3. Temperature and stress profile used for T-TRIP investigations.

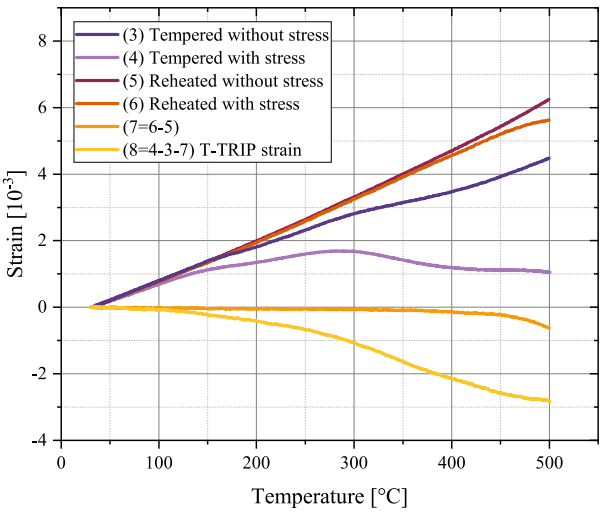

Fig. 4. Different determined curves for the separation of T-TRIP strain according to [6].

2.3. Separation of T-TRIP strain

For further analysis of the T-TRIP effect it was necessary to separate the corresponding proportion of the strain ε_{TRIP} from the total measured strain. This evaluation was carried out by a method developed by Kaiser [6].

Firstly, the samples tempered without any applied stress have a total strain of

$$\varepsilon_{t0} = \varepsilon_{pt} + \varepsilon_{th} \tag{3}$$

where ε_{pt} corresponds to the strain due to phase transformation and ε_{th} the thermal strain.

Secondly, the amount of total strain for samples tempered under applied stress is

$$\varepsilon_{tot} = \varepsilon_{pt} + \varepsilon_{th} + \varepsilon_{el} + \varepsilon_{cr} + \varepsilon_{TRIP} \tag{4}$$

where ε_{el} is the elastic strain of the dilatometric setup, ε_{cr} the creep strain and ε_{TRIP} the TRIP strain.

In the next step, the same tempering step without any stress is repeated for all samples which have been tempered under stress. As the phase transformation has already taken place during the first experiment, this new total strain only consists of the thermal strain:

$$\varepsilon_{rh0} = \varepsilon_{th} \tag{5}$$

At last, each sample is tempered under stress for a second time, leading to the following strain:

$$\varepsilon_{rh} = \varepsilon_{th} + \varepsilon_{el} + \varepsilon_{cr} \tag{6}$$

Subtracting Eq. (5) from Eq. (6) gives

$$\varepsilon' = \varepsilon_{rh} - \varepsilon_{rh0} = \varepsilon_{el} + \varepsilon_{cr}. \tag{7}$$

Using the previously calculated and measured strains, it is possible to separate T-TRIP strain:

$$\varepsilon_{TRIP} = \varepsilon_{tot} - \varepsilon_{t0} - \varepsilon' \tag{8}$$

Fig. 4 shows the corresponding curves for each tempering step.

2.4. Microstructural and mechanical characterization

Vickers microhardness was measured using a Qness Q10A+ according to the standard DIN EN ISO 6507-1 [18]. Indentation time was set to 10 s and the measurements were carried out with $HV_{0.1}$ due to the small cross section of dilatometric samples. Martensitic and tempered samples were verified regarding constant hardness in the length direction. For the hardness measurements after TRIP experiments, both dilatometric samples were additionally cut in the middle perpendicular to the length axis.

Table 2
Measured yield strength of the investigated steels under compression and tension at $T_t = 500\,°C$, as well as the calculated SD.

	σ_{yC} [MPa]	σ_{yT} [MPa]	SD [%]
25CrMo4	−558 ± 8	417 ± 17	25
34CrMo4	−486 ± 7	406 ± 13	16
50CrMo4	−506 ± 32	397 ± 33	21

A Zeiss Leo Gemini 1530 scanning electron microscope (SEM) was used for the microstructural characterization of the carbides. SEM samples were prepared in the longitudinal direction in order to analyze the influence of stress. They were ground, polished, and etched with 2%-Nital prior to the investigations. The ImageJ [19] plugin Trainable WEKA Segmentation [20] has been used to analyze SEM images using artificial intelligence (AI). A classifier is trained and used to distinguish the precipitates from the matrix. Subsequently, the segmented image is binarized and the precipitates surface area percentage (PSAP) is calculated, using the function Analyze Particle. The mean value is calculated from at least a total of 10 images per sample, because the distribution of cementite precipitates is not homogeneous for low carbon steels [21]. For each steel, two samples were analyzed: one with no stress and one with $0.5 \cdot \sigma_y$. Finally, a PSAP mean value from both samples has been calculated for determining the dependency on the TRIP constant. Furthermore, using the MorphoLibJ plugin [22] on binarized images, the connected components were labeled and analyzed with respect to their orientation.

3. Results

3.1. Tensile and compression tests

As mentioned in Section 2.2, compression and tensions tests at the tempering temperature of 500 °C were carried out for all three steels using the dilatometer. The compression and tensile yield strengths were measured and later used to avoid exceeding half the yield strength, in order to stay in the range where the relationship between ε_{TRIP} and stress is linear. The results, as well as the occurring SD between compression and tensile tests, are listed in Table 2.

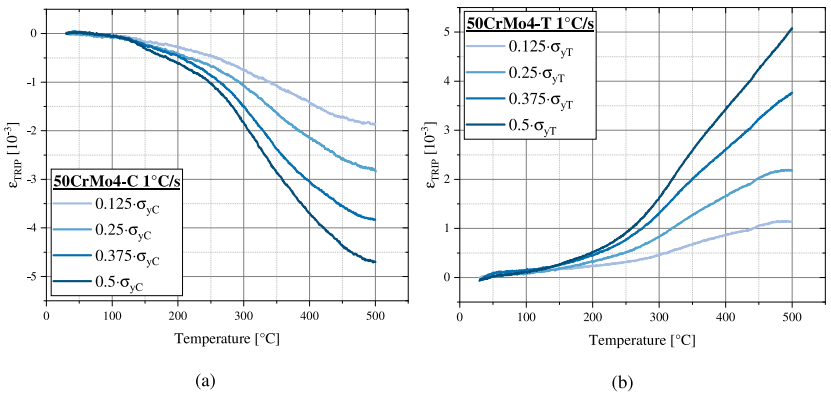

Fig. 5. Evolution of T-TRIP strain during continuous tempering up to 500 °C with 1 °C/s for 50CrMo4 under (a) compression and (b) tension stress.

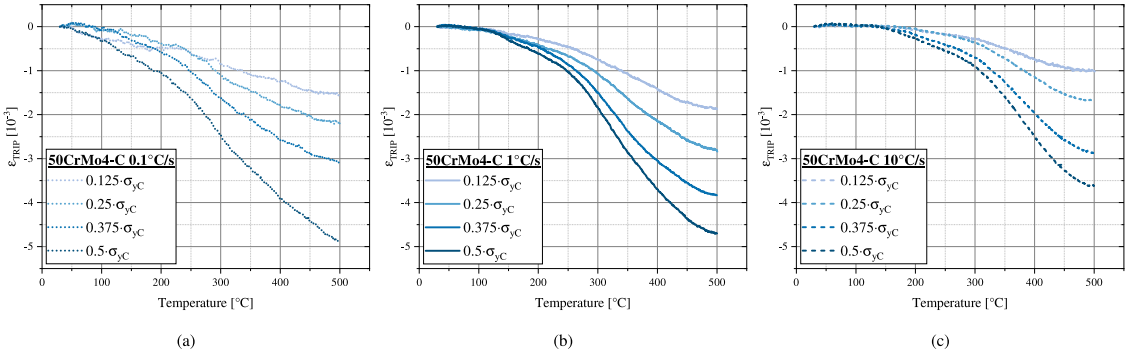

Fig. 6. Evolution of T-TRIP strain during continuous tempering up to 500 °C for 50CrMo4 with (a) 0.1 °C/s, (b) 1 °C/s and (c) 10 °C/s.

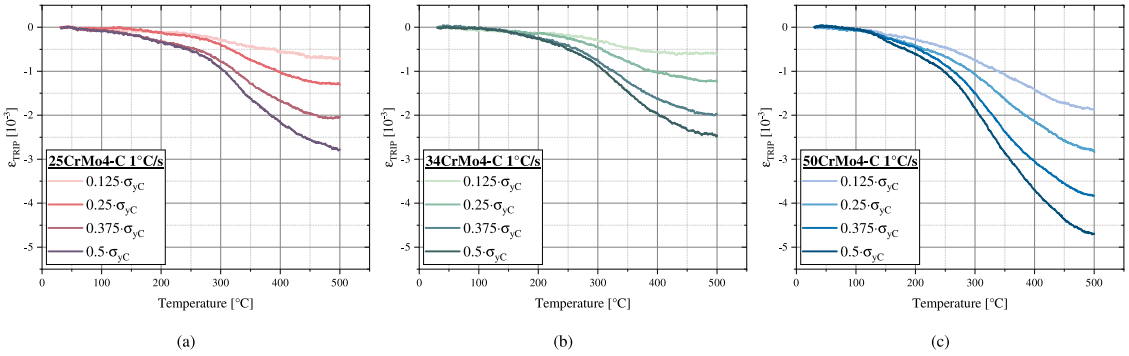

Fig. 7. Evolution of T-TRIP strain during continuous tempering up to 500 °C with 1 °C/s for (a) 25CrMo4, (b) 34CrMo4, and (c) 50CrMo4 under compression stress.

3.2. TRIP during tempering

Using dilatometric experiments, as well as the method mentioned in Section 2.3, ε_{TRIP} was calculated from the measured ε_{tot}. To gain a better understanding of the dependencies of T-TRIP on different parameters, the following factors have been varied: stress level, stress direction, heating rate, and amount of Carbon in the investigated steel. The results will be presented in the subsections below. The experiment on 50CrMo4 under compression stress and with a heating rate of 1 °C/s has been used as a reference for the variation of the parameters.

3.2.1. Influence of the stress level and direction

Fig. 5 shows the evolution of ε_{TRIP} during tempering with 1 °C/s up to 500 °C under different compression (labeled with C) and tension (labeled with T) stresses up to $0.5 \cdot \sigma_y$. Increasing the stress leads to the growth of $|\varepsilon_{TRIP}|$ under both compression and tension stress. As expected, the strain is always in the same direction as the applied stress (negative under compression and positive under tension).

3.2.2. Influence of the heating rate

Fig. 6 shows the variation of ε_{TRIP} for 50CrMo4 during the tempering with heating rates 0.1 °C/s, 1 °C/s and 10 °C/s up to 500 °C under compression. The higher heating rate (10 °C/s) leads to the lowest maximum values of $|\varepsilon_{TRIP}|$. However, the lowest heating rate (0.1 °C/s) does not always lead to a higher $|\varepsilon_{TRIP}|$ at T_t. In contrast, the values of $0.125 \cdot \sigma_y$, $0.25 \cdot \sigma_y$ and $0.375 \cdot \sigma_y$ are even lower than those of the samples heated with 1 °C/s.

3.2.3. Influence of the carbon content

The evolution of ε_{TRIP} for the three investigated Q&T steels is shown in Fig. 7, all corresponding to tempering up to 500 °C with a heating rate of 1 °C/s. The observed augmentation of ε_{TRIP} with higher stresses for 50CrMo4 is also visible for the other steels. While the maximum value of $|\varepsilon_{TRIP}|$ under a stress of $0.5 \cdot \sigma_y$ varies between $2 \cdot 10^{-3}$ and $3 \cdot 10^{-3}$ for 25CrMo4 and 34CrMo4, it rises up to $5 \cdot 10^{-3}$ in case of 50CrMo4.

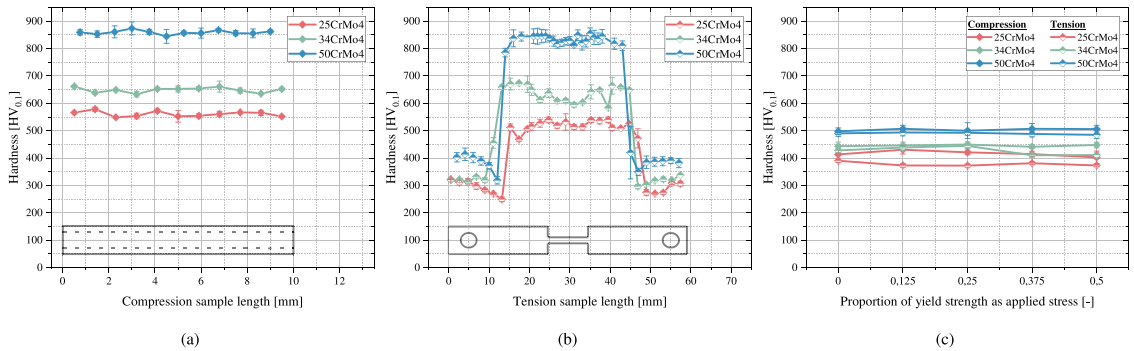

Fig. 8. Measured hardness of the quenched martensitic sample for (a) compression and (b) tension experiments as well as (c) the achieved hardness after tempering with 1 °C/s under different applied stresses.

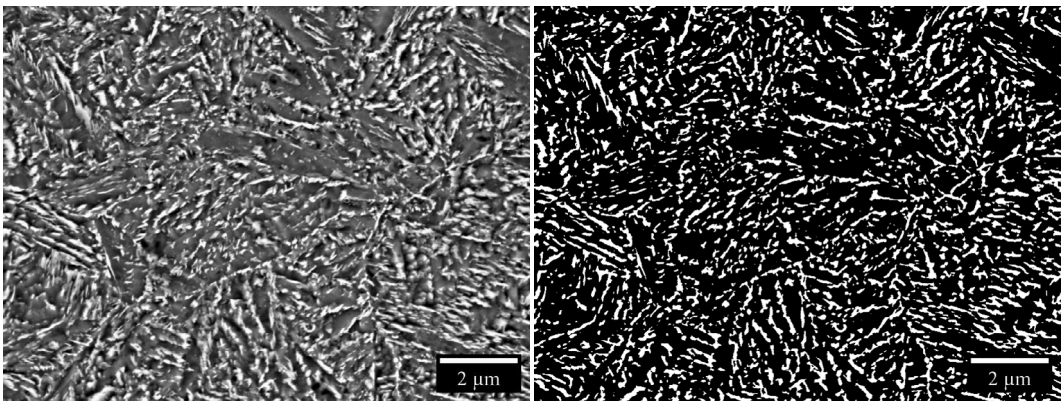

Fig. 9. (a) Original SEM image from the sample 50CrMo4-C under 0 MPa, as well as (b) the binarized image using trainable WEKA segmentation tool.

3.3. Hardness measurements

To verify if the samples are homogeneously heat treated in the length direction, both geometries were subject to hardness measurements after quenching. The hardness values for these martensitic samples are shown in Figs. 8(a) and 8(b). In both samples the hardness of martensite rises with the amount of C in steel. Due to the structure of the dilatometer, the tension sample cannot be completely hardened, but the relevant section in the middle, where the length change is measured, has only slightly lower values than the compression sample. Nevertheless, both samples are homogeneously hardened in the length change measurement area. Same tendencies were observed for tempered samples. Fig. 8(c) shows the hardness of compression and tension samples after tempering under different applied stresses. It is notable that the stress level and thus the T-TRIP strain have no influence on the hardness. The higher amount of C in 50CrMo4 has led to the highest hardness after tempering; however, the difference between the three steels is not as pronounced as in the quenched state.

3.4. Microstructural investigations

Fig. 9 shows one example of the microscopic investigation by means of SEM. Fig. 9(a) is the original image from the 50CrMo4-C sample with 0 MPa. Cementite is distinguishable by its lighter color due to the etching. It is mostly at low-angle or high-angle grain boundaries, and long carbide chains are visible on lath edges. Fig. 9(b) is the binary image obtained using the WEKA segmentation tool, by the method described in Section 2.4. The precipitates surface area percentage (PSAP), which corresponds to the white areas in the image, was calculated for all samples and the results are shown in Fig. 10. The determined mean values are listed in Table 3.

Table 3
Mean values of PSAP for different SEM samples tempered under compression (Ø PSAP-C) and tension (Ø PSAP-T).

Material	Heating rate [°C/s]	Ø PSAP-C [%]	Ø PSAP-T [%]
25CrMo4	1	8.6 ± 1.9	8.1 ± 2.6
34CrMo4	1	9.1 ± 2.6	9.9 ± 1.9
50CrMo4	1	15.2 ± 4.8	10.8 ± 0.8
50CrMo4	0.1	12.8 ± 4.0	–
50CrMo4	10	10.7 ± 1.9	–

It must be said that different samples, although etched at the same time for the same duration, might react differently to the etchant, and therefore this uncertainty should be considered when comparing the results. In most of the cases, the sample tempered under stress has a lower PSAP than that tempered without applied stress. There is no significant tendency when comparing compression and tension samples. When the heating rate is kept constant, the PSAP rises with the amount of C, but this effect is more pronounced for the compression samples than the tension samples. The variation in the heating rate for 50CrMo4-C samples had a significant influence on PSAP in samples tempered without stress. Consequently, when comparing the PSAP mean values, 10 °C/s leads to the lowest amount of precipitates, which was predictable due to the shorter precipitation time. However, the slowest heating rate of 0.1 °C/s also leads to a lower PSAP than the sample with 1 °C/s.

Furthermore, the analysis of the orientation distribution of the precipitates by MorphoLibJ described in Section 2.4 has been carried out, but the samples under stress did not show any preferred orientation in the applied stress direction.

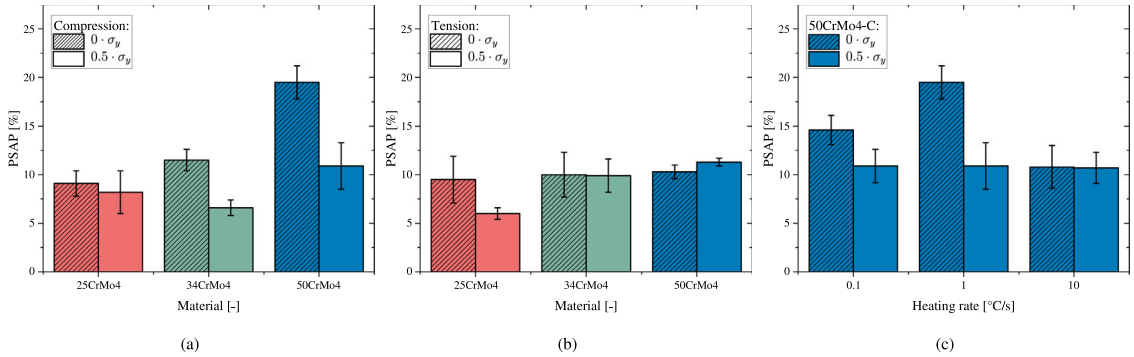

Fig. 10. Measured PSAP after tempering with and without applied stresses for (a) compression samples with a heating rate of 1 °C/s, (b) tension samples with a heating rate of 1 °C/s and (c) 50CrMo4 compression samples with different heating rates.

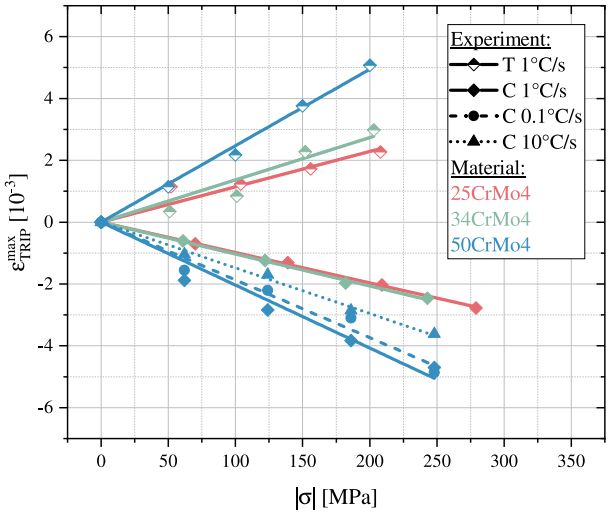

Fig. 11. The dependency of maximum TRIP strain on the applied stress, as well as the corresponding T-TRIP constant K for the three Q&T materials.

Table 4
Measured TRIP constants after tempering up to T_i for the investigated Q&T steels under compression (K_C) and tension (K_T).

Material	Heating rate [°C/s]	$\lvert K_C \rvert$ $\left[10^{-6}\frac{1}{\text{MPa}}\right]$	$\lvert K_T \rvert$ $\left[10^{-6}\frac{1}{\text{MPa}}\right]$
25CrMo4	1	9.9 ± 0.2	11.4 ± 1.0
34CrMo4	1	10.0 ± 0.2	13.7 ± 1.3
50CrMo4	1	20,4 ± 1.1	24.7 ± 0,6
50CrMo4	0.1	18,7 ± 0.9	–
50CrMo4	10	14.7 ± 0.3	–

4. Discussion

The results have shown the dependencies of different variables on the amount of TRIP strain after continuous tempering up to 500 °C. To describe the T-TRIP effect more generally and integrate it into modeling and simulations, the TRIP constant K is calculated. Fig. 11 shows the maximum TRIP strain ε_{TRIP}^{max} at 500 °C depending on the applied stress for each material. The linear fit for each set of points delivers K. The determined TRIP constants under compression stress (K_C) and tensile stress (K_T) are listed in Table 4 for each material.

Fig. 12(a) shows the dependence of $|K|$ on the amount of carbon in steel after tempering with 1 °C/s. Steels with a higher amount of C contain an elevated amount of cementite [21], therefore $|K|$ was expected to increase with a higher amount of carbon. However, the increase is not linear and lower carbon contents (0.26% and 0.35%) rather build a plateau, whereas there seems to be an exponential growth of $|K|$ for 0.49% carbon. Furthermore, the tension samples tend to have a slightly higher $|K|$ than the compression samples. This can eventually be due to different sample geometries, which might have an influence on the sample heat transfer. Therefore, the heat treatment might not be exactly the same under compression and tension. Such factors have a direct influence on the microstructure, and thus on the T-TRIP strain. However, since these aspects cannot be taken into account in a correlation of $|K|$ with the carbon content, a more generally valid correlation is required in order to predict $|K|$ for different material states. Consequently, further analysis has been carried out on the relationship between $|K|$ and the surface area percentage of precipitates (PSAP), which has led to consistent results, even with variation in the heating rate and direction of stress. Fig. 12(b) shows that, except for one outlier sample (50CrMo4-T 1 °C/s), there is a direct linear dependency of $|K|$ on PSAP.

Fig. 13 shows a SEM image from the outlier sample 50CrMo4-T 1 °C/s tempered under stress. Orange circles show examples of areas where the precipitates could not be recognized by the AI-based segmentation, which could explain the low calculated PSAP compared to the expected trend. The reason may be the uncertainties regarding the different reactions of each sample to the etchant, which causes different outcomes in the gray scale of the precipitates.

It must also be mentioned that PSAP was expected to reduce with increasing heating rate [23], yet it was not the case for the sample with 0.1 °C/s. It should be considered that PSAP only considers a 2D surface and larger precipitates may not be considered correctly in the PSAP. But even though the PSAP of the sample with 0.1 °C/s heating rate is between those with 1 °C/s and 10 °C/s, this does not change the conclusions for $|K|$, and thus the tendencies agree.

It can be concluded that carbon content cannot be used as a reliable parameter to describe the dependence of K, but it is rather the size and amount of the precipitates which plays an important role. These observations indicate that the Greenwood–Johnson mechanism is the dominant effect. It demonstrates that the volume change is responsible for the measured TRIP strain. No orientation effect was observed by means of SEM, indicating that the Magee effect has no visible influence during tempering. Further microstructural studies are necessary to verify if the precipitates exhibit any differences in their morphology when tempered under stresses compared to without stresses, for example by analyzing the stress fields around the precipitates by means of transmission electron microscopy. Nevertheless, a linear dependence of $|K|$ on PSAP could be demonstrated and can serve as a basis for further investigations. Moreover, it is necessary to adapt existing approaches from the literature for the modeling of TRIP as a function of the temperature and stress to the tempering phase transformation.

5. Conclusion

Dilatometric studies, alongside mechanical and microstructural characterizations were carried out to investigate the transformation

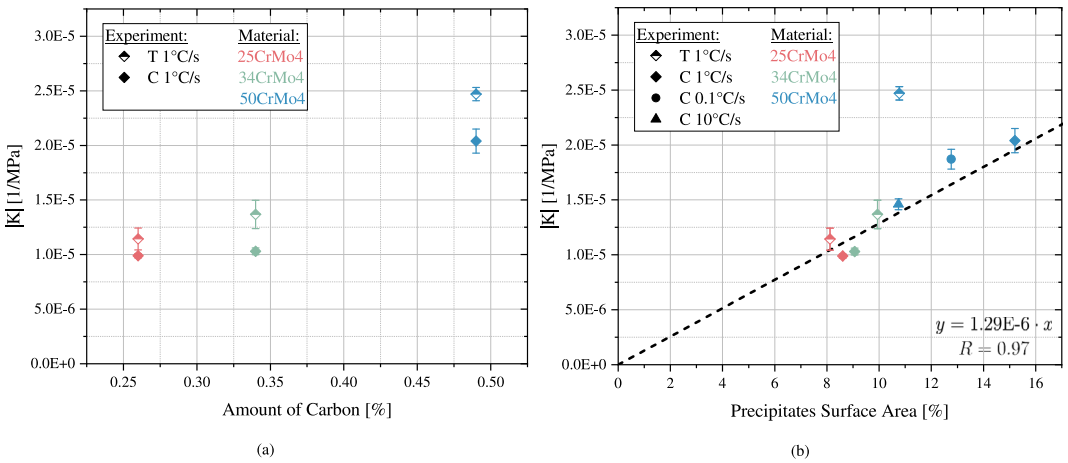

Fig. 12. Different T-TRIP constants under tension and compression and their corresponding (a) amount of carbon, as well as (b) surface area percentage of the precipitates (PSAP), including the linear fit describing the dependency of K on PSAP.

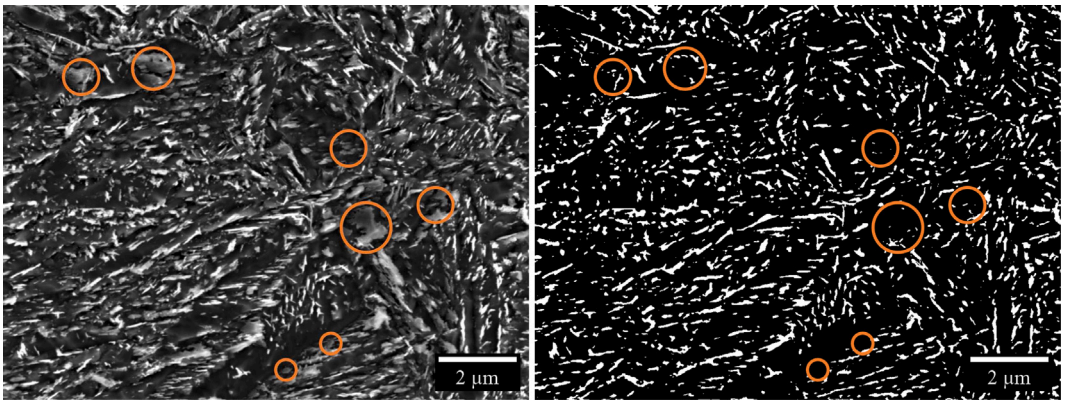

Fig. 13. (a) Original SEM image from the sample 50CrMo4-T under $0.5 \cdot \sigma_y$ stress, as well as (b) the binarized image using trainable WEKA segmentation tool. Orange circles showcase some examples of single precipitates or a cluster of them, which were not recognized by AI during the segmentation. (For interpretation of the references to color in this figure legend, the reader is referred to the web version of this article.)

induced plasticity (TRIP) during tempering of quenched and tempered (Q&T) steel. The following summarizes the main findings of this study.

- The study successfully demonstrated the TRIP effect during continuous tempering (T-TRIP) across three distinct Q&T steels, evidenced in both tension and compression testing.
- Despite the T-TRIP effect, there was no observed change in hardness when comparing samples tempered with and without applied stress.
- Further analysis revealed a linear correlation between the modulus of TRIP constant $|K|$ and the precipitates surface area percentage, which itself is dependent on a variety of factors such as carbon content and heating rate. This indicates the presence of Greenwood–Johnson effect during tempering.

In further investigations, these results could be used as a basis to verify T-TRIP in a real application, for example by tempering samples which already contain residual stresses due to surface hardening.

Fundings

This work was supported by the German Research Foundation (Deutsche Forschungsgemeinschaft, DFG) with the project number 428958028.

Declaration of competing interest

The authors declare that they have no known competing financial interests or personal relationships that could have appeared to influence the work reported in this paper.

Acknowledgments

Special thanks go to Dr. James Damon and Dr. Fabian Mühl from Institute for Applied Materials – Materials Science and Engineering (IAM-WK) for assistance in conducting dilatometric investigations and their insightful discussions throughout the project. Additionally, the authors express their gratitude to Dr. Alexander Kauffmann from Institute for Applied Materials – Materials Science and Engineering (IAM-WK) for his support in the SEM investigations.

References

[1] Schwenk M, Hoffmeister J, Schulze V. Experimentally validated residual stresses and distortion prediction for dual frequency induction hardening. Int J Appl Electromagn Mech 2014;44(2):127–35. http://dx.doi.org/10.3233/JAE-141752, Num Pages: 9.

[2] Habschied M, Graaff B, Klumpp A, Schulze V. Fertigung und eigenspannungen. HTM J Heat Treat Mater 2015;70(3):111–21. http://dx.doi.org/10.3139/105.110261.

[3] Fischer FD, Sun Q-P, Tanaka K. Transformation-Induced Plasticity (TRIP). Appl Mech Rev 1996;49(6):317–64. http://dx.doi.org/10.1115/1.3101930.
[4] Greenwood GW, Johnson RH. The deformation of metals under small stresses during phase transformations. Proc R Soc Lond Ser A Math Phys Sci 1965;283(1394):403–22. http://dx.doi.org/10.1098/rspa.1965.0029.
[5] Magee CL, Paxton HW. Transformation kinetics, microplasticity and aging of martensite in Fe-31Ni. 1966, Place: Carnegie Institute of Technology, Pittsburgh, PA.
[6] Kaiser D, Graaff B, Jung AM, Dietrich S, Schulze V. A dilatometric study on the influence of compressive stresses on the tempering of martensitic AISI 4140 steel - Evidence of transformation induced plasticity during cementite precipitation. Mater Sci Eng A 2017;705:114–21. http://dx.doi.org/10.1016/j.msea.2017.08.028, Num Pages: 8.
[7] Kaiser D, Damon J, Mühl F, Graaff B, Kiefer D, Dietrich S, Schulze V. Experimental investigation and finite-element modeling of the short-time induction quench-and-temper process of AISI 4140. J Mater Process Technol 2020;279:116485. http://dx.doi.org/10.1016/j.jmatprotec.2019.116485.
[8] Abrassart F. Influence des transformations martensitiques sur les propriétés mécaniques des alliages du système Fe-Ni-Cr-C (Ph.D. thesis), 1972.
[9] Wolff M, Böhm M, Dalgic M, Hüßler I. Evaluation of models for TRIP and stress-dependent transformation behaviour for the martensitic transformation of the steel 100Cr6. Comput Mater Sci 2008;43(1):108–14. http://dx.doi.org/10.1016/j.commatsci.2007.07.040.
[10] Leblond JB. Mathematical modelling of transformation plasticity in steels II: Coupling with strain hardening phenomena. Int J Plast 1989;5(6):573–91. http://dx.doi.org/10.1016/0749-6419(89)90002-8.
[11] Besserdich G. Untersuchung zur eigenspannungs-und verzugsausbildung beim abschrecken von zylindern aus den stählen 42 crMo4 und ck45 unter berücksichtigung der umwandlungsplastizität (Ph.D. thesis), Universität Karlsruhe; 1993.
[12] Sjöström S. The calculation of phase transformation and residual stresses resulting from quenching of steel. Numer Method Therm Probl 1985;1189–202.
[13] Desalos Y. Comportement dilatométrique et mécanique de l'austénite métastable d'un acier A533. IRSID Rep 1981;95349401.
[14] Köhler W. Atlas der Wärmebehandlung der Stähle, herausgegeben vom Max - Planck - Institut für Eisenforschung in Zusammenarbeit mit dem Werkstoffausschuß des Vereins Deutscher Eisenhüttenleute. Teil 1: v. Wever-Rose; Teil 2: v. Rose-Peter-Straßburg. Form DIN A4; 147. Mater Corros 1955;6(12). http://dx.doi.org/10.1002/maco.19550061217, 612–612.
[15] Speich GR, Leslie WC. Tempering of steel. Metall Trans A 1972;3(5):1043–54. http://dx.doi.org/10.1007/BF02642436.
[16] Läpple V. Wärmebehandlung des Stahls: [Grundlagen, Verfahren und Werkstoffe], 9., aktualisierte Aufl.. Bibliothek des technischen Wissens, Haan-Gruiten: Verl. Europa-Lehrmittel Nourney, Vollmer; 2006.
[17] Ellermann A, Scholtes B. The strength differential effect in different heat treatment conditions of the steels 42CrMoS4 and 100Cr6. Mater Sci Eng A 2015;620:262–72. http://dx.doi.org/10.1016/j.msea.2014.10.027.
[18] DIN EN ISO 6507-1, Metallische Werkstoffe - Härteprüfung nach Vickers - Teil 1: Prüfverfahren. 2018, http://dx.doi.org/10.31030/2778746, Issue: DIN EN ISO 6507-1.
[19] Schneider CA, Rasband WS, Eliceiri KW. NIH Image to ImageJ: 25 years of image analysis. Nat Methods 2012;9(7):671–5. http://dx.doi.org/10.1038/nmeth.2089.
[20] Arganda-Carreras I, Kaynig V, Rueden C, Eliceiri KW, Schindelin J, Cardona A, Sebastian Seung H. Trainable Weka Segmentation: a machine learning tool for microscopy pixel classification. Bioinformatics (Oxford, England) 2017;33(15):2424–6. http://dx.doi.org/10.1093/bioinformatics/btx180.
[21] Zhao M, Hanamura T, Qiu H, Nagai K, Yang K. Dependence of strength and strength-elongation balance on the volume fraction of cementite particles in ultrafine grained ferrite/cementite steels. Scr Mater 2006;54(7):1385–9. http://dx.doi.org/10.1016/j.scriptamat.2005.11.067.
[22] Legland D, Arganda-Carreras I, Andrey P. MorphoLibJ: integrated library and plugins for mathematical morphology with ImageJ. Bioinformatics 2016;32(22):3532–4. http://dx.doi.org/10.1093/bioinformatics/btw413.
[23] Revilla C, López B, Rodriguez-Ibabe J. Carbide size refinement by controlling the heating rate during induction tempering in a low alloy steel. Mater Des 2014;62:296–304. http://dx.doi.org/10.1016/j.matdes.2014.05.053.